Structure of APP-C99$_{1-99}$ and implications for role of extra-membrane domains in function and oligomerization

George A. Pantelopulos[a], John E. Straub[a,*], D. Thirumalai[b], Yuji Sugita[c]

[a] Department of Chemistry, Boston University, 590 Commonwealth Avenue, Boston, MA 02215-2521, USA
[b] Department of Chemistry, The University of Texas, Austin, TX 78712-1224, USA
[c] Theoretical Molecular Science Laboratory, RIKEN, 2-1 Hirosawa, Wako-shi, Saitama 351-0198, Japan

ARTICLE INFO

ABSTRACT

The 99 amino acid C-terminal fragment of Amyloid Precursor Protein APP-C99 (C99) is cleaved by γ-secretase to form Aβ peptide, which plays a critical role in the etiology of Alzheimer's Disease (AD). The structure of C99 consists of a single transmembrane domain flanked by intra and intercellular domains. While the structure of the transmembrane domain has been well characterized, little is known about the structure of the flanking domains and their role in C99 processing by γ-secretase. To gain insight into the structure of full-length C99, REMD simulations were performed for monomeric C99 in model membranes of varying thickness. We find equilibrium ensembles of C99 from simulation agree with experimentally-inferred residue insertion depths and protein backbone chemical shifts. In thin membranes, the transmembrane domain structure is correlated with extra-membrane structural states and the extra-membrane domain structural states become less correlated to each other. Mean and variance of the transmembrane and G$_{37}$G$_{38}$ hinge angles are found to increase with thinning membrane. The N-terminus of C99 forms β-strands that may seed aggregation of Aβ on the membrane surface, promoting amyloid formation. In thicker membranes the N-terminus forms α-helices that interact with the ni-castrin domain of γ-secretase. The C-terminus of C99 becomes more α-helical as the membrane thickens, forming structures that may be suitable for binding by cytoplasmic proteins, while C-terminal residues essential to cytotoxic function become α-helical as the membrane thins. The heterogeneous but discrete extra-membrane domain states analyzed here open the path to new investigations of the role of C99 structure and membrane in amyloidogenesis. This article is part of a Special Issue entitled: Protein Aggregation and Misfolding at the Cell Membrane Interface edited by Ayyalusamy Ramamoorthy.

1. Introduction

Amyloid Precursor Protein (APP), a 770-residue membrane protein, plays important roles in neural activity and regulation of synaptic formation [1]. The canonical APP processing pathway is defined by APP cleavage by either α- or β-secretase resulting in 83- or 99-residue long peptides (C83 and C99), that form the majority of APP fragments in cells [2]. C99 can subsequently undergo processive cleavage of its transmembrane domain by γ-secretase at various sites within its transmembrane (TM) region, yielding 38, 40, 42, and 43-residue long N-terminal fragments commonly known as Amyloid β (Aβ) protein [3]. Aβ$_{42}$ (and to some extent Aβ$_{43}$) has been implicated in the onset of Alzheimer's disease (AD) due to the presence of fibrillar aggregates enriched in these peptides [4,5] found in the brains of AD patients [6]. In addition, Aβ$_{42}$ oligomers have been directly observed to accompany loss of neural plasticity and memory [7].

Solution NMR measurements [7,8] employing zwitterionic lipid bicelles and micelles provide the primary source of information on the structure of C99 in a variety of membrane mimicking environments. In these in vitro environments, there is evidence that residues 1–14 (see Fig. 1) of the N-terminal domain (NTD) are disordered, residues 15–25 of the N-terminus have helical propensity (N-Helix), residues 26–28 form a turn (N-Turn), residues 29–52 form the helical transmembrane domain (TMD), residues 53–90 of the C-terminus form a disordered region (C-Loop), and residues 91–99 of the C-terminus form a helix (C-Helix) [8,9]. Insertion of residues in the membrane evidenced by EPR [8] and NMR [9] measurements suggest that in some systems the C-Helix and N-Helix domains rest on the membrane surface, while the proximities of the NTD and C-Loop domain to the membrane remain unclear.

The structure of the TMD is believed to be critical to the mechanism of recognition and cleavage of C99 by γ-secretase. The process of
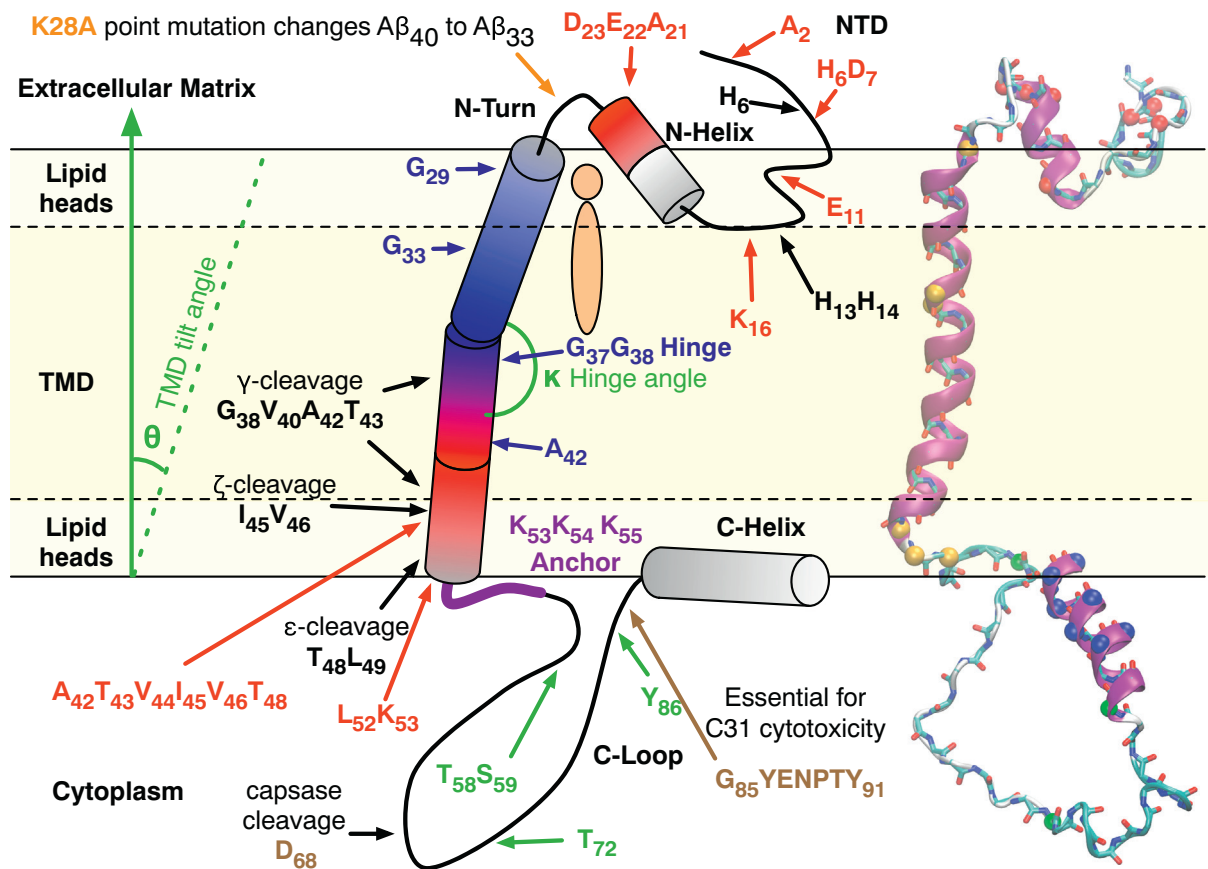
Fig. 1. Yellow shading represents hydrophobic core of the membrane. Red residues contain familial AD mutations. Blue residues are critical to the formation of C99 dimers. Green residues may be phosphorylated. Purple residues form the lysine anchor. Black residues indicate γ-secretase cleavage sites and metal binding residues. Brown residues are critical for C31 formation and cytotoxicity. Cylinders represent domains with significant helical propensity. θ and κ angles describe the TMD tilt and GG hinge angle. The θ angle increases with thinning or curving of the membrane surface, and κ increases with curving of the membrane surface. Black solid lines mark the membrane surface and black dashed lines represent the membrane hydrophobic core. The orange lipid marks the putative cholesterol binding site. Also shown is an atomistic structure of C99 predicted from TALOS + using LMPG micelle backbone chemical shifts and secondary structure assigned with STRIDE. Cα within the atomistic structure are labeled as N-terminal familial AD mutation (red), residues 28, 37, 38, 53,54, and 55 (orange), phosphorylatable residues Cα (green), and C-Helix (blue).

cleavage of C99 by γ-secretase begins with the "ε-cleavage" step, forming Aβ$_{48}$ or Aβ$_{49}$, which are then further cleaved via "ζ-cleavage" to form Aβ$_{45}$ and Aβ$_{46}$. These fragments are subsequently processed by "γ-cleavage" to predominantly form Aβ$_{38}$ or Aβ$_{42}$, and Aβ$_{40}$ or Aβ$_{43}$, respectively [10]. C99 features a glycine zipper motif, G$_{29}$xxxG$_{33}$xxxG$_{37}$, in the TMD, which is frequently observed in dimer-prone single-pass TM proteins [11,12]. It is further evidenced to be a component of putative cholesterol binding site on C99 [13,14], a finding that is important because cholesterol has been hypothesized to recruit C99 to γ-secretase [14–16]. Mutation of G$_{29}$ and G$_{33}$ in this motif reduces Aβ$_{42}$ production [17], and is expected to reduce C99 dimerization [18]. Proximate to the N-terminal portion of the GxxxG repeat motif lies a "GG hinge" at G$_{37}$G$_{38}$ in the TMD, previously identified by molecular dynamics simulations [19,20] and conjectured to be important to processing by γ-secretase [21]. Hydrogen-deuterium (H-D) exchange studies observed side chain [21] and α-helix [22] hydrogen bonds to be substantially weaker near the GG hinge, suggesting the amide bonds are readily available for γ-cleavage. Thickening of the membrane reduces the relative amount of Aβ$_{42}$ and Aβ$_{43}$ produced while leading to an overall increase in γ-secretase activity [23,24]. Increasing the curvature of membrane is found to increase the magnitude of fluctuation of the GG hinge and the overall tilt of the TMD [25]. It is likely that magnitude of fluctuations in the hinge may enhance Aβ$_{42}$ and Aβ$_{43}$ production [8]. Additionally, simulation studies have revealed [20,26,27] that the GG hinge is an important structural feature

for C99 dimers, with the angle of the hinge varying for several distinct dimerization motifs. It has further been noted that the membrane thickness can preferentially stabilize and environmentally select specific C99 dimer structures [17,26–28]. Beyond the hinge lies G$_{38}$xxxA$_{42}$, another glycine zipper motif often found in TM dimers [18], important for C99 homodimerization [29]. The GxxxG repeat motif appears to facilitate C99 dimer formation in thicker membranes while the competing GxxxA motif supports dimers that are most often observed in thinner membrane and micelle [30]. At the C-terminal end of the TMD, residues A$_{42}$, T$_{43}$, V$_{44}$, I$_{45}$, V$_{46}$, T$_{48}$, L$_{52}$, and K$_{53}$ all feature several mutations found in AD [31]. Some mutations decrease the propensity for homodimerization [32], and enhance Aβ$_{42}$ production [33]. A "lysine anchor" formed by the triple repeat K$_{53}$K$_{54}$K$_{55}$ is evidenced to register at the C-terminal end of the TMD membrane surface [34].

While the TMD structure has been the focus of experimental and computational studies, the structure of the extra-membrane residues has received relatively little attention in spite of the evidence that changes to the extra-membrane domains of C99 are crucial to determining the production of Aβ and onset of AD. The N-terminus of C99 almost certainly interacts with the nicastrin domain of γ-secretase [35]. Within the N-Loop domain, Ala point mutation of K$_{28}$ has a dramatic impact on APP processing, switching formation of Aβ$_{40}$ to Aβ$_{33}$, implicating this turn in the γ-secretase interaction [34]. Residues 15 to 21 (LVFFAED of the N-Helix domain), sometimes referred to as the juxta-membrane (JM) region, plays a role in inhibiting γ-secretase binding

[36] and binding with cholesterol [8,13,15]. Furthermore, membrane insertion of residues in the JM region appears to sensitively depend on pH [13]. The N-Helix also features mutants A21G [37], E22Q [38], E22K [39], E22G [40], E22Δ [41], and D23N [42], all found to occur in AD patients. Within the NTD, the mutation K16N is known to make APP untenable for binding by α-secretase [43,44] and the E11K mutation was found to enhance Aβ production [45]. The mutations D7H [46], D7N [47], H6R [47], and A2V [48] were found in patients with early onset of AD, suggesting a role for these residues in interaction with γ-secretase. Additionally, histidine residues in the N-terminus H_6, H_{13}, and H_{14} are known to bind with Cu and Zn metals, found in high concentration in amyloid plaques [49]. Additionally, $Aβ_{42}$ forms a complex with the C99 N-terminus when C99 is membrane-bound, which enhances C99 homo-oligomer formation [50].

In the C-Loop there are several phosphorylatable residues, identified at T_{58}, S_{59}, T_{72} [46], and Y_{86} [51]. The phosphorylation of S_{59} enhances trafficking of APP to the Golgi apparatus [52]. It has been noted that Ala point mutation at T_{72} may enhance the production of $Aβ_{40}$ and $Aβ_{42}$ [53–55], impacting interaction of APP with some enzymes [56]. Y_{86} has been identified to be phosphorylated at higher concentrations in the brains of AD patients, and is suspected to prevent the interaction of APP with adaptor proteins [54].

The C-Loop and C-Helix are known to interact with several proteins in the cytoplasm, forming complexes in which these domains adopt an α-helical structure [57]. The C99 sequence binds to many cytoplasmic proteins including the G protein G0 with residues H_{61}-K_{80} [58], the adaptor protein Fe65 with residues D_{68}-N_{99} [59], the adaptor protein X11 with residues Q_{83}-Q_{96} [60], the adaptor protein mDab1 with a similar residues to X11 [61], and the kinase Jip-1with residues N_{84}-F_{93} [62]. The C-terminus is cleaved by caspases at D_{68} to form C31, a cytoplasmic protein found in AD patients and evidenced to signal apoptosis [63]. Aβ-C99 complex-enhanced C99 oligomerization increases the production of C31 [50]. Mutation of D_{68} to Ala prevents production of C31, abrogating cytotoxic function [64]. Additionally, residues 85–91 (GYENPTY) are found to be essential for cytotoxic activity of C31, and are involved in interactions with many cytoplasmic proteins [50].

Currently, the experimental knowledge of extra-membrane residues of C99 is limited to backbone chemical shifts and NOEs measured in LMPG micelles, EPR signals measured in POPC:POPG membranes, and hydrophobic and hydrophilic NMR probe signals in membrane-mimicking detergent bicelles, for which the structural ensembles of residues 6, 12–16, 53–56, 62, 73–76, 80, 81, and 88 are unresolved or too uncertain [8,9]. A prodigious body of work characterizing structure of Aβ fragments has been performed and generally suggests that residues 21–28 of Aβ act as a seed for oligomerization and fibril formation. It has been conjectured that this region contains key residues characterizing the aggregation-prone N^* state of Aβ and Aβ fragments [65,66]. Support for this conjecture has been provided by NMR and computational studies of $Aβ_{40}$ and $Aβ_{42}$ structural ensembles [67]. Additionally, the N-Turn and C-Loop domains show nearly random coil chemical shifts, implying that they are unstructured on average. However, these domains may exhibit heterogeneity of metastable structural states as has been observed in many intrinsically disordered proteins. The current knowledge of C99 structure and residue features in typical thermodynamic conditions is summarized in Fig. 1.

To address some of the outstanding questions related to the structure of C99 and its interaction with the membrane we performed simulations of monomeric wildtype C99 in model membranes, using a computational approach that proved to be remarkably useful in elucidating structures of the TMD [19,20,27]. We employed replica-exchange molecular dynamics (REMD) [68] to sample hundreds of nanoseconds of C99 dynamics at physiological temperatures in 30, 35, and 40 Å-thick membranes modeled using the GBSW implicit solvation method [69].

In thin membranes we observed extracellular domain states to be correlated with the TMD state. The mean and variance of the TMD and GG hinge angles (Fig. 1) were observed to increase with thinning of the membrane. The C- and N-terminal secondary and tertiary structures of C99 were heterogeneous with discrete metastable states which we found to become increasingly correlated as the membrane thickens. These ensembles were directly compared and contrasted with the results of prior solution NMR and EPR studies [8,9]. C99 ensembles were found to exhibit newly-observed metastable α-helical and β-strand structures in C- and N-termini, which are correlated with the state of the TMD only in thin membranes. β-Strand structures observed in some N-terminal residues are suggestive of templates that may seed amyloid oligomerization on the membrane surface. α-Helical domains in the N-terminus are observed and found to be suggestive of nicastrin association sites. α-Helical domains observed in previously uncharacterized phosphorylatable sites T_{58}, S_{59}, and Y_{86} (see Fig. 1), suggest that these domains may be involved in interactions that enhance the phosphorylation processes. Overall, our work provides insight into the structure of extra-membrane residues of C99 and lays the foundation for further investigations considering the role of C99 structure in facilitating intermolecular interactions in membrane.

2. Methods

2.1. Initial structure preparation

We constructed an initial structure of the full-length C99 sequence using current literature data. Residues 23–55 were modeled using a "Gly-in" structure of one C99 sampled in the recent work by Dominguez et al. [27] Onto this fragment, residues 1–22 and 56–99 were built using dihedral angles predicted via the TALOS+ [70], using the Cα, Cβ, C, N, and H chemical shifts reported for C99 in LMPG micelles [30]. To remove clashes and effectively move the C-Helix close to the membrane surface, the ψ angle of H_{14}, located in the disordered loop of the N-terminus (see Fig. 1), was adjusted to 180° and the φ angle of Q_{82} was adjusted to 180°. The rotomeric states of residues 1–22 and 56–99 were assigned using the Shapovalov and Dunbrack rotamer library [71]. Protonation states were assigned using the AddH program in UCSF Chimera [72], assigning negative GLU and ASP, positive LYS and ARG, neutral CYS and TYR, and setting HIS to the HSD CHARMM histidine type. The center of the membrane was defined by the z-coordinate of the Cα of G_{38}.

2.2. Molecular dynamics simulation

All simulations were performed using CHARMM version c41b1 [73] using the CHARMM36 force field [74], likely to be the most accurate force field for simulation of Aβ [75]. The GBSW implicit membrane solvent model was used [69], employing a 0.004 kcal/mol Å^{-2} surface tension, 5 Å smoothing length from the membrane core-surface boundary, and 0.6 Å smoothing length at the water-membrane surface boundary, using 24 radial and 38 angular integration points to 20 Å. No cutoffs were used for nonbonded interactions. After C99 was inserted in 30, 35, and 40 Å-thick implicit membranes the potential energy was minimized using the steepest descent algorithm until apparent convergence, and simulated for 130, 160, and 460 ns, respectively, using REMD [68] via the REPDSTR utility in CHARMM. We used 16 replicas in REMD simulations, employing exponentially-spaced temperatures from 310 to 500 K and attempting to exchange temperature conditions every 1 ps, manifesting an overall exchange success rate of 17.7 ± 3.7%. Langevin dynamics was employed using a 2 fs time step with a leap frog integrator, a 5 ps^{-1} friction constant, and constrained hydrogen bonds via the SHAKE algorithm. Atomic coordinates were written every 10 ps and all analyses employed coordinate data at this resolution.
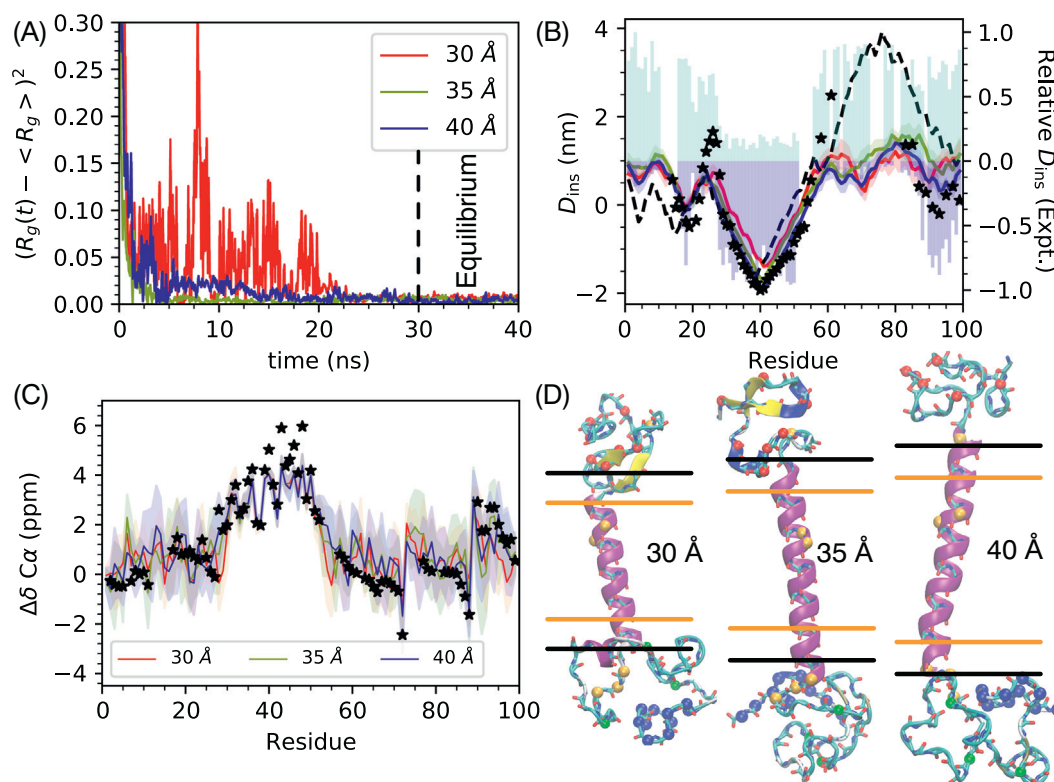
Fig. 2. (A) Squared difference of *Rg* from ensemble average over time. The vertical dashed line at 30 ns demarcates the time beyond which the ensembles are considered to be at equilibrium. (B) Equilibrium average and standard deviation of insertion depth of residue Cα in the membrane, D_{ins}. Stars indicate scaled relative depths of residue insertion to the membrane inferred from EPR probe signals in POPG:POPC membranes, dashed line represents insertion depths of the initial C99 structure in a 35 Å membrane [8]. Scaled NMR signals from lipophilic (blue) and hydrophilic (cyan) probes in POPC-DHPC bicelles shown in bars [9]. (C) Equilibrium average and standard deviation of Cα chemical shifts predicted using SHIFTX2. Stars indicate the Cα chemical shifts measured in LMPG micelles. (D) Structures of C99 at 30 ns in 30, 35, and 40 Å membranes. (Same residue coloring as in Fig. 1).

2.3. Analysis methods

SciPy [76,77], Cython [78], Matplotlib [79], VMD v1.9.3 [80], MDAnalysis v.0.16.2 [81,82], MDtraj v1.9.0 [83] were employed for analyses. SHIFTX2 was used to compute the full set of chemical shifts of C99 in each frame for thermodynamic conditions of 7.4 pH and 310 K temperature [84]. All analyses considered structures sampled at equilibrium (past 30 ns) in the 310 K ensemble from REMD. To assign conformational states of extra-membrane domains of C99, a relatively low-dimensional space that enables precise clustering was constructed. Secondary structure assignments were made using the STRIDE implementation in VMD.

To cluster C99 structures four Principal Component Analysis (PCA) eigenspaces were constructed, using Cα positions and the sine and cosine transformations of dihedral angles (dPCA [85]) of N-terminal residues 1–29 and C-terminal residues 52–99, using data from the equilibrium ensemble in 30, 35, and 40 Å membranes. The first 3 principal components of simulation data in each of these four eigenspaces were considered relevant, each conformation of C99 described by a 12-dimensional space capturing the secondary and tertiary structure of the N- and C-terminus. Conformations at each membrane thickness were assigned to states by clustering in this 12-dimensional space using a Gaussian Mixture Model (GMM). The GMMs were constructed for simulations at each membrane thickness using *k*-means clustering to parameterize initial clustering and weights of each data point in each cluster, then refined using 100 iterations of the GMM Expectation-Maximization algorithm [86]. We aimed to construct GMMs that would provide a precise clustering of the most significant conformational states while separating rarely sampled states to small clusters. This was determined by performing Akaike information criterion (AIC) and

Bayesian information criterion (BIC) tests on GMM models constructed of 1–30 clusters, which suggest that 30 or more clusters would be an ideal model of the system states (Fig. S1). We first noted that the mean in the AIC and BIC appear at 8 clusters in 30, 35, and 40 Å membranes. We then built 16-cluster GMM models such that rare conformations were separated from the 8 most-populous clusters, and validated the precision of these clusters by visual inspection of all assigned conformations. Metric multidimensional scaling of the 12-dimensional data to 2 dimensions for each membrane thickness was performed in order to visualize the nature of the clustering and the relative distance between states.

To measure the correlation between the N- and C-terminal domains of C99, we cluster the N- an C-terminus separately using the same input data used for the combined clusters of N- and C-terminal domains, constructing N- and C-terminal domain 16-cluster GMMs in 30, 35, and 40 Å membranes. We measured the normalized mutual information

$$\frac{\sum_C^M \sum_N^M p(N,C) \log \frac{p(N,C)}{p(N)p(C)}}{\sqrt{\left(\sum_N^M p(N) \log p(N)\right)\left(\sum_C^M p(C) \log p(C)\right)}},$$

(1)

where *M* is the number of clusters, *p(N)* is the likelihood of the *Nth* N-terminus cluster, *p(C)* is the likelihood of the *Cth* C-terminus cluster, and *p(N,C)* is the joint probability of the *Nth* and *Cth* cluster, which ranges from 0 to 1, 1 representing maximum correlation between the N- and C-terminus state changes.
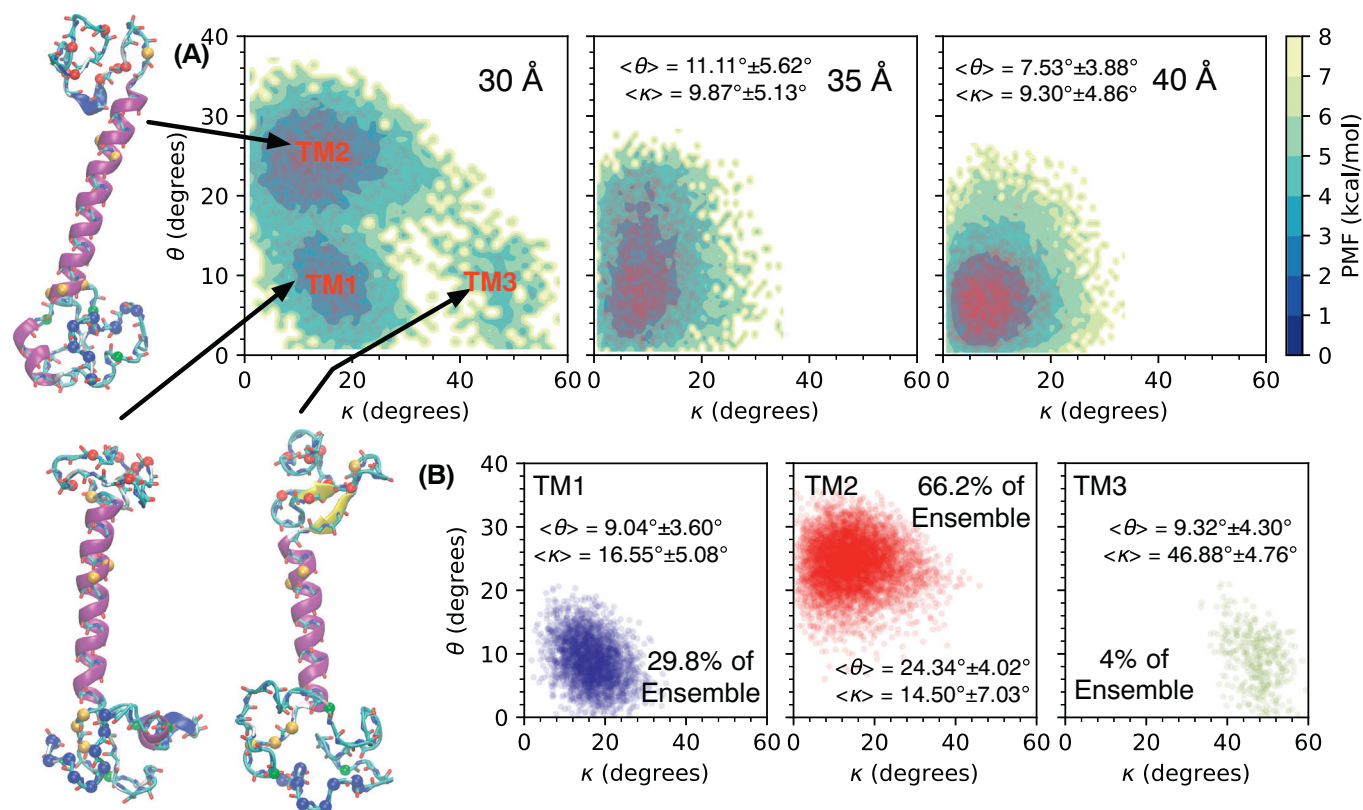
Fig. 3. TMD (θ) and GG kink (κ) angles of C99 (A) PMF ($-k_BT \ln(p)$) at equilibrium in 30, 35, and 40 Å membranes, showing 4000 randomly selected data points in red and (B) 30 Å membrane for TMD macrostates TM1 (blue), TM2 (red), and TM3 (gold), which compose 66.2, 29.8, and 4% of the equilibrium ensemble, respectively. Insets show mean and standard deviation of angles in the displayed macrostate. Representative C99 conformation secondary structure drawn with STRIDE and Cα colored as defined in Fig. 1.

3. Results and discussion

3.1. Convergence of ensemble to equilibrium and experiment

Full C99 sequence was simulated using REMD in GBSW implicit membranes, a successful approach for enhanced sampling of membrane protein structure [87]. Membranes of 30, 35, and 40 Å thicknesses, corresponding to lipids of 12-, 14-, and 16-carbon sn-1 lipid tails, such as DLPC, DMPC, and POPC, respectively, were used to study the effect of membrane structure on the conformational ensemble of C99 [88]. The initial structure of C99, constructed from a combination of past simulations and chemical shift-based dihedral assignments (Fig. 1), gradually evolved in REMD simulations to interact with the membrane surface. The radius of gyration (R_g) rapidly converged to the ensemble average in 35 and 40 Å membranes, but appeared to require 20 ns to converge in 30 Å membranes due to relatively slow re-arrangements in secondary structure near the membrane surface (Fig. 2A), evidenced by deep insertion of C99 to the membrane. We considered the equilibrium ensemble to have been reached by 30 ns in all REMD simulations, and only consider data at equilibrium for characterization of C99 structure.

The ensemble average of Cα residue depths of insertion (D_{ins}) in the membrane were well-captured by simulation, comparing well with NMR signals from hydrophobic and hydrophilic probes in POPC-DHPC bicelles and correlating with past EPR measurements in POPG:POPC membranes (40 Å-thick membranes) by Pearson's r of 0.888, 0.861, and 0.894 for 30, 35, and 40 Å membranes, respectively (Fig. 2B). This is substantially better than the initial structure of C99 prepared for these simulations, which has a Pearson's r correlation with these EPR insertion depths of 0.717, deviating most in the C-terminus. This marginally higher insertion depth correlation observed in 40 Å membrane may be attributed to the insertion of the C-Helix in the membrane surface. The

whole sequence of the C-Helix was observed to rest on the membrane surface in much of the 40 Å ensemble in contrast with the 30 and 35 Å ensembles that predominantly show residues around T_{90} to rest on the membrane surface. The higher correlation of C99 residue insertion in 40 Å implicit membranes is coincident with POPC membrane, which has been measured to be approximately 40 Å thick in combined analysis of small-angle neutron and X-ray scattering data [88]. The significant deviations in insertion depth at residue 60 seem to suggest that these implicit membrane simulations cannot capture structural features of C99 unique to POPC:POPG membranes, as POPG lipids carry a net negative charge and these implicit membrane simulations attempt to model zwitterionic lipids.

Cα chemical shifts predicted using the SHIFTX2 algorithm, which boasts the best correlations of predicted chemical shifts to experiment of current chemical shift prediction methods, show substantial correlation with those measured in LMPG micelles (r correlation coefficients of 0.882, 0.908, and 0.903 for 30, 35, and 40 Å membranes) (Fig. 2C). However, overall the 40 Å membrane simulations showed higher correlation with all backbone chemical shifts (Fig. S2 and Table S1) [30]. Deviations from the LMPG experimental chemical shifts suggest that C99 is slightly too helical in residues 55–70. Furthermore, the degree of lower correlation observed of 30 Å membranes stems from lower propensity for helical structure in residues 90–99. The secondary structure propensities of each residue in conformational states of the extramembrane region are discussed in further detail in Section C.

3.2. TMD tilt and hinge angles

The hinge located at $G_{37}G_{38}$ has been conjectured to modify the interaction of C99 with γ-secretase in a way that impacts C99 processing [21]. As the membrane thickness increases the production of Aβ
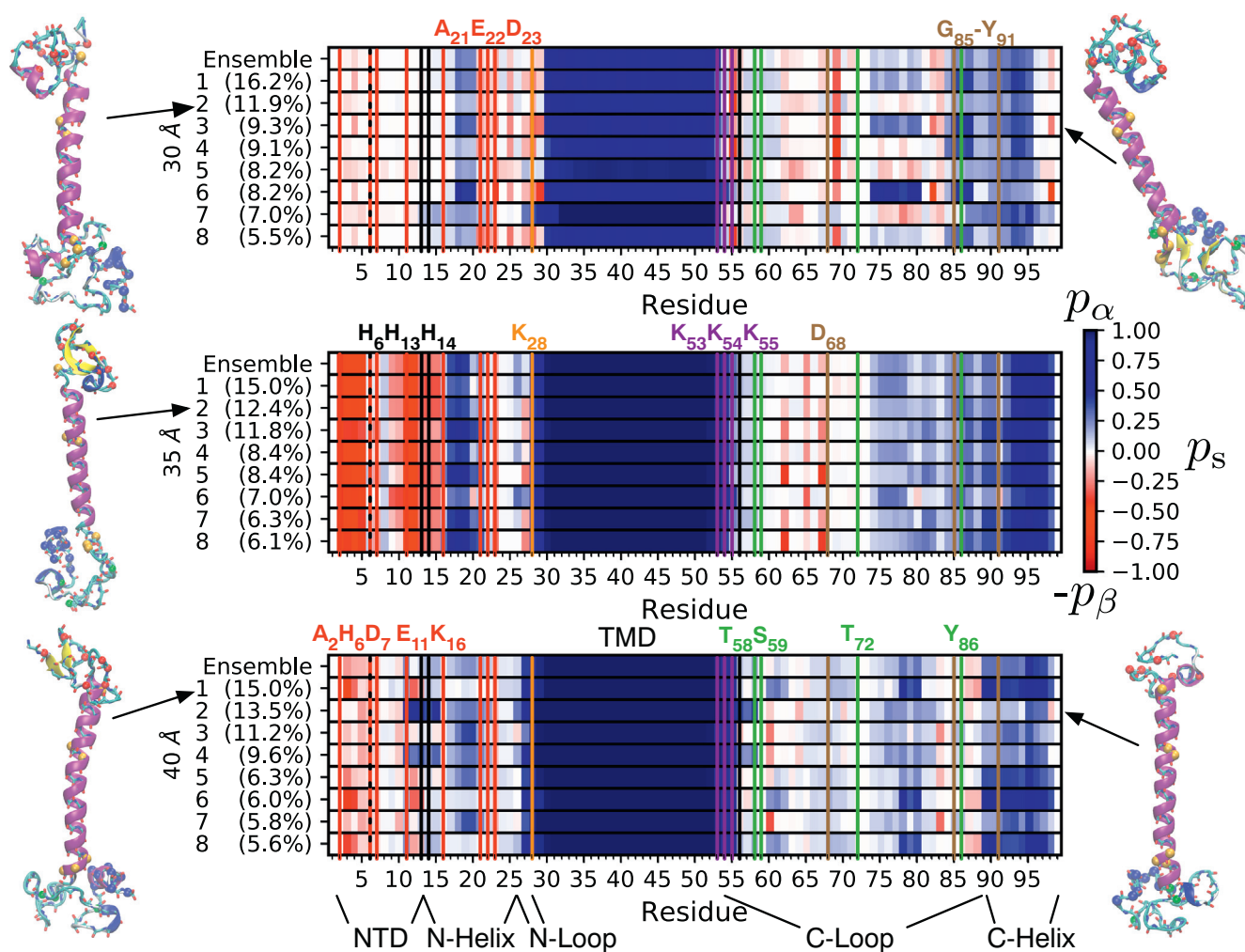
Fig. 4. Difference of α and β propensity at each C99 residue in the ensemble (see scale for secondary structure propensity on the right) and in the 8 most populous clusters in 30, 35, and 40 Å membranes (percentages correspond to population of the ensemble). Lines and text indicate residue indices of interest: AD-associated mutations (red), phosphorylation sites (green), lysine anchor (purple), metal binding sites (black), Aβ₃₃-producing mutation (orange), and C31 cleavage and cytotoxic function sites (brown). Last frame of visualized C99 clusters with secondary structure drawn with STRIDE and Cα shown as in Fig. 1.

has been reported to increase overall, but the ratio of Aβ₄₂/Aβ₄₀ decreases [23,24]. This suggests that C99 structures in thick membranes are preferable for appropriate interactions of C99 and γ-secretase. The stability of the TMD helix at the GG hinge has been observed to be weaker than the rest of the TMD via H-D exchange experiments [21,22].

In past simulation studies, the GG hinge flexibility did not appear to be sensitive to membrane thickness [27]. However, the simulations presented here include the full C99 sequence, which seems to be important for sampling certain TMD structures (Fig. 3). We define the TMD tilt angle (θ) as the angle between the vector of best fit through residue 30–52 Cα positions and the z-axis (Fig. 1). The GG hinge angle (κ) is the angle between the vectors of best fit through Cα positions of residues 30–37 and of residues 38–52 (Fig. 1). In 40 Å membranes there is a single macrostate of TMD structure with average and standard deviation in TMD angles ($<\theta>$) of $7.5° \pm 3.9°$ and GG hinge angles ($<\kappa>$) of $9.3° \pm 4.9°$. In 35 Å membranes these angles increase to $<\theta> = 11.1° \pm 5.6°$ and $<\kappa> = 9.9° \pm 5.1°$. In 30 Å membranes three structural macrostates of the TMD are observed, composing 29.8% (TM1), 66.2% (TM2), and 4.0% (TM3) of the ensemble. Extra-membrane clusters 4, 5, 7, and 8 comprise TM1, featuring $<\theta>$ of $9.1° \pm 3.6°$ and $<\kappa>$ of $16.6° \pm 7.0°$. Clusters 1, 2, 3, 6, 9, 10, 12, 13, 14, 15, and 16 comprise TM2, which exhibits $<\theta>$ of $24.3° \pm 4.0°$ and $<\kappa>$ of $14.5° \pm 7.0°$. Cluster 10 comprises TM3, characterized by $<\theta>$ of $9.3° \pm 4.3°$ and $<\kappa>$ of $46.9° \pm 4.8°$. The

extreme hinge bend in TM3 is an artifact, resulting from unraveling of TMD residues 31–33 to form a β-strand with residues 20–22. We also analyzed the PMF along θ in the 30 Å membrane discarding the TM3 state, finding the energy barrier between TM1 and TM2 to appear at $\theta = 16°$ with approximately 3 kcal/mol, while the basin of TM1 appears at $\theta = 8°$ with approximately 2.3 kcal/mol and the basin of TM2 appears at $\theta = 25°$ with approximately 1.8 kcal/mol (Fig. S3.)

These observations suggest that the mean and variance of TMD and GG hinge angles generally increase as a result of membrane thinning. The increase is accompanied by considerable heterogeneity in the C99 structures. In future experiments, these results might be experimentally verified using aligned lipid bilayers with solid-state NMR, RDC solution NMR, or TROSY NMR in bicelles.

### 3.3. Secondary structure, membrane insertion, and implications of C99 states

The secondary and tertiary structures of extra-membrane residues in C99 are observed to be heterogeneous. Using projection of simulation data onto a 12-dimensional space the describing relevant PCA eigenvectors of secondary and tertiary structures of N- and C-terminal extra-membrane residues, conformational clusters were assigned and refined using k-means and a Gaussian Mixture Model to find the 16 conformational states defined in 30, 35, and 40 Å membranes (Figs. S4–6).

These clusters were inspected by embedding the 12-dimensional space to a 2-dimensional space by metric multidimensional scaling and viewing all assigned atomistic structures (Figs. S7–9). The correlation in changes to the conformation state of the N- and C-terminal domains was evaluated by constructing 16-cluster GMMs of these domains independently using the same structural information and calculating the normalized mutual information of N- and C-terminal domain cluster assignments (Eq. (1)). We found the correlation between domains to be 0.596, 0.634, and 0.854 in 30, 35, and 40 Å membranes, increasing with membrane thickness.

Considering the 8 most populated clusters of each membrane, which account for 75.4, 75.4, and 73.0% of 30, 35, and 40 Å membrane ensembles, we identify the most prominent C99 states. Secondary structure assignment via STRIDE allows for the general classification of structure. We consider the secondary structure propensity by taking the difference between the observed α-helix likelihood (p_α) and the observed β-strand likelihood (p_β) ($p_s = p_\alpha - p_\beta$) for each cluster, such that when $p_s = +1$ the residue has complete α-helical propensity and when $p_s = -1$ the residue has complete β-strand propensity (Fig. 4). In each membrane condition, we observe unique secondary structures including or proximal to sites of non-TMD familial AD mutations, phosphorylatable sites, and the metal binding sites. To consider tertiary structure we measured the insertion depth of Cα to the membrane surface (D_{ins}) (Fig. 5).

The TMD is observed to lengthen on both the C- and N-terminal ends with increasing membrane thickness. The TMD was extended by two residues at the N-terminus and one residue at the C-terminus every 5 Å increase in membrane thickness, growing from residues 30–53 in 30 Å membranes to residues 26–55 in 40 Å membranes. This observation is in contrast to the usual assumption [34] that the lysine anchor does not change its registration with the membrane surface, and that only the N-terminal end of the TMD changes registration with the membrane surface as membrane thickness changes. This had previously been unconfirmed, as past experiments on full-length C99 could not resolve structure or membrane insertion of the lysine anchor in a variety of environments [9]. Residue K_{28}, found to change production of $A\beta_{40}$ to $A\beta_{33}$ when mutated to Ala [34], is incorporated in the TMD helix, undergoing a transition from β to α structure as membrane thickness increases.

In all membrane conditions residues 16–20 have helical propensity and are inserted in the membrane, in agreement with prior EPR and NMR experiments, and comprise the helix previously observed from residues 13–23 in past solution-phase Aβ NMR experiments [89]. The full C-Helix, identified as being inserted in membrane in past experiments, is found to be helical in all conditions other than 30 Å, for which residues 96–99 are unstructured and unassociated with the membrane surface. The C-Helix is observed to be helical even when unassociated with the membrane surface, a condition observed in some clusters in all
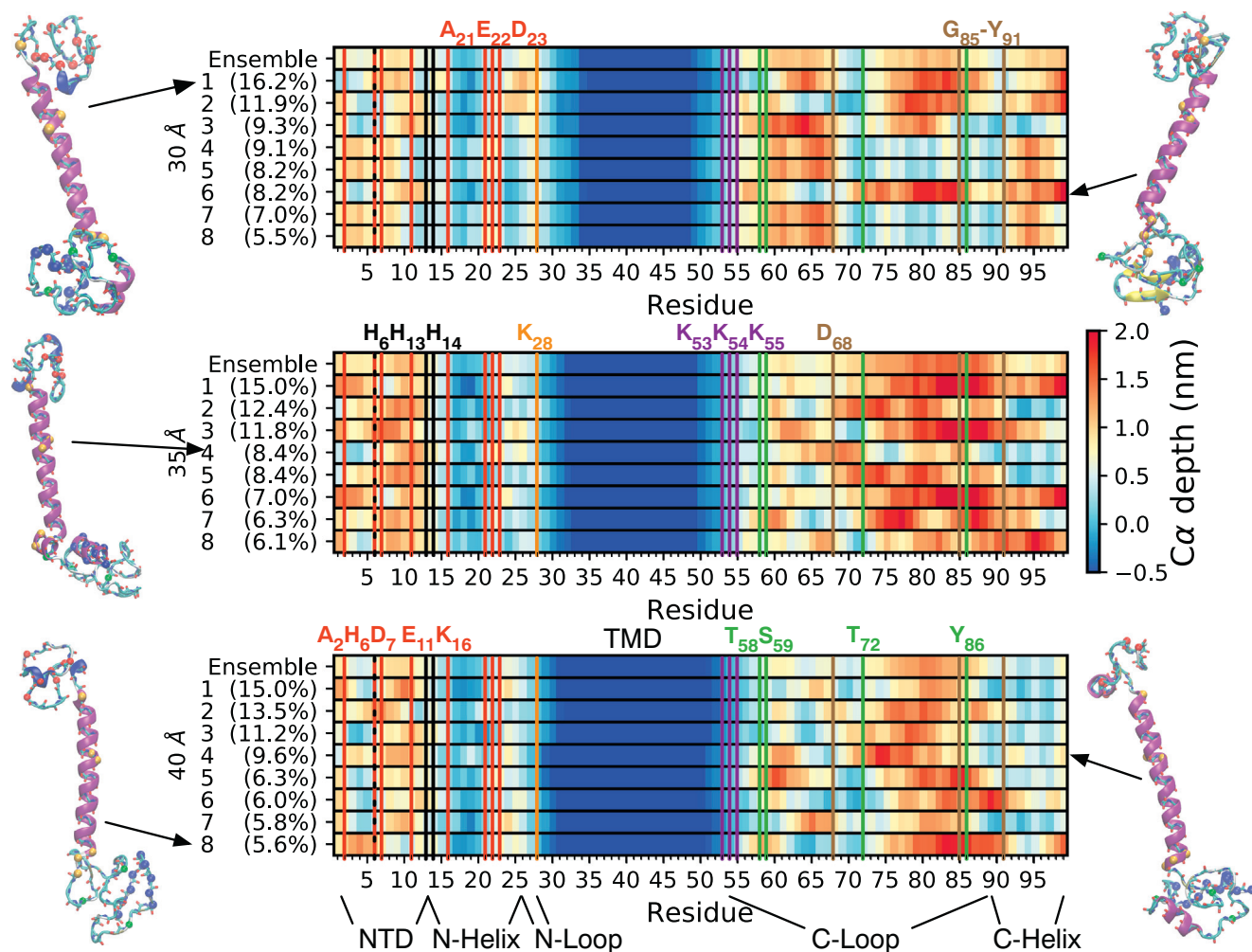
Fig. 5. Average membrane insertion of each C99 residue Cα ensemble (see scale for depth of insertion on the right) in the ensemble and in the 8 most populous clusters in 30, 35, and 40 Å membranes (percentages correspond to population of the ensemble). Lines and text indicate residue indices of interest: AD-associated mutations (red), phosphorylation sites (green), lysine anchor (purple), metal binding sites (black), Aβ_{33}-producing mutation (orange), and C31 cleavage and cytotoxic function sites (brown). Last frame of indicated C99 clusters with secondary structure drawn with STRIDE and Cα shown as in Fig. 1.

membrane conditions. This finding provides a structural basis for the conjecture that the C-Helix is available for binding with cytoplasmic proteins in any membrane condition. Residues 73–76, for which membrane insertion and chemical shifts had been previously unresolved in NMR experiments with micelles and bicelles, as well as in EPR experiments with membranes, appear to be unstructured in all membranes and broadly distributed relative to the membrane surface. Residues 74 to 80 are found to be slightly less helical and more bound to the membrane surface in 30 Å membranes, suggesting that thinner membranes may make C99 less available for binding to the G0 protein, which binds residues 61–80 [58]. Residue D_{68}, the cleavage site for cytotoxic C31 peptide formation, gains more β-propensity in thinner membranes. The cytotoxic functional domain G_{85}-Y_{91} becomes more α-helical in response to membrane thinning, though the insertion depth does not follow a trend, being membrane-associated in 30 and 40 Å, and membrane-disassociated in 35 Å membranes. It may be possible that C99 in thinner membranes is more amenable to cleavage of D_{68} to form C31.

In 30 Å membranes, residues 21–23, 25–27, and 28–30 occasionally interact to form β-strands, suggestive of the aggregation-prone N^* structural motif observed in Aβ fragments [65,66]. This structure is not present in 35 and 40 Å membranes, in which residues 28–30 join the TMD helix. Mutants of residues 21–23 are featured in cases of familial AD and thin membranes are known to cause an increase in the ratio of $Aβ_{42}/Aβ_{40}$ produced. It is possible that mutations in residues 21–23 stabilize this β-strand, altering the TMD ensemble to resemble the structure observed in 30 Å membranes. Additionally, in some clusters, residue K_{55} forms H-bonds consistent with β-strand structures involving A_{69}, occasionally including Q_{82} and Q_{83} as well.

In 35 Å membranes, a prominent β-hairpin is formed with residues 2–5 and 11–15, in which residue N_{27} sometimes participates via H-bonding. This hairpin is positioned away from the membrane surface. This structure does not appear in membrane-bound $Aβ_{1-42}$ in similar implicit membrane simulations [20], and seems to be unique to 35 Å-thick membranes. It is possible that this β-hairpin structure acts as a seed for Aβ oligomerization. C99-seeded Aβ association to the membrane may be much more favorable than pure Aβ mixtures considered in the past [90], as Aβ is at substantially higher concentration outside the cells than in the membrane. Mutation of residues 2, 11, and 16, found in familial AD, may change the propensity for this β-hairpin to form. Additionally, H_6, H_{13}, and H_{14}, residues known to bind metal ions found at high concentration in amyloid plaques [49] are proximate to the observed β-hairpin. The structure of His-ion complexes found in computational investigations of $Aβ_{1-16}$ resembles this hairpin structure [91,92]. As such it may be possible that 35 Å membranes are ideal for stabilizing C99 structures that bind metal ions.

In 40 Å membranes there is weaker propensity for β-hairpin formation observed in 35 Å membranes. A strand with residues 2–5 and 11–13 in some clusters, such as 1, 6, and 8, is observed. In clusters 2 and 4, residues 11–15 form an α-helix that is unassociated with the membrane. Along with residues 16–20, this helix may serve as an interaction site with the nicastrin domain of γ-secretase. The formation of these α-helices may serve to enhance the recognition of C99 by γ-secretase as one possible mechanism explaining the observed increase in Aβ processing observed in thicker membranes.

The secondary structure propensities and insertion depth of non-TMD residues 1–28 and 52–99 for the whole ensemble and for each cluster reveal that the helicity of extra-membrane residues is not correlated with membrane insertion depth. This observation is contrary to the typical expectation that the hydrophobic membrane environment increases the propensity for helical structure. This is quantified by Pearson's r correlation of non-TMD residue secondary structure propensity to membrane insertion of Cα, $r(p_s, D_{ins})$, in the ensemble and in clusters (Fig. 6). It is possible that this could be a consequence of the simulation model used, and further investigation using explicit solvent simulations with consideration of the disordered protein structure
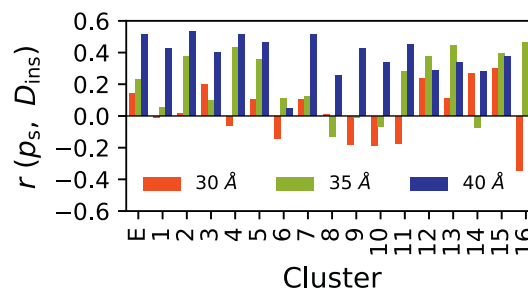

Fig. 6. Pearson's r correlation of average Cα depth of insertion in membrane (D_{ins}) and difference in observed α and β structure propensity (p_s) in C99 residues 1–28 and 53–99 in the equilibrium ensemble (E) and in each cluster.

should be pursued.

4. Conclusions

We performed REMD simulations of full length C99 in model membranes of 30, 35, and 40 Å thicknesses. Heterogeneous but discrete structural states observed in the C99 C– and N-terminal extra-membrane regions of C99 are found to be unique to the specific membrane condition. This observation supports past work on C99 congeners in lipid bilayers [25–27] in which the specific lipid composition, membrane thickness, and membrane curvature were observed to impact C99 monomer and dimer structure. We observe that the TMD and $G_{37}G_{38}$ hinge angle means and variances increase as the membrane becomes thinner. Multiple TMD states were observed in thin membranes which were found to be directly correlated with the conformational state of extra-membrane domains. Generally, an increase in α and β secondary structure is observed as membrane thickness increases, accompanied by an increasing correlation between changes in N- and C-terminal domain conformational states. The TMD helix expands on the N- and C-terminal ends as membrane thickness increases. Residues 21–23, 25–27, and 28–30 form β-strands similar to the aggregation-prone N^* motif previously observed in Aβ fragments in 30 Å membranes. In addition, residues 2–5 and 11–15 form a β-hairpin in 35 Å membranes. It is conjectured that these β-strand motifs may serve as seeds for Aβ aggregation on the membrane surface. Residues 11–15 adopt α-helical structures in 40 Å membranes that may promote binding of C99 with the nicastrin domain of γ-secretase to promote non-amyloidogenic processing of C99. α-Helical structures are generally stabilized in the C-terminus as membrane thickness increases, and do not require association with the membrane surface. This observation suggests that these domains are readily available to interact with proteins in the cytoplasm. Conversely, residues 85–91, known to be essential to cytotoxic function, become α-helical as the membrane thins. These observations drawn from our simulation study are summarized in Fig. 7.

The insights provided by this study enhance our understanding of the structural ensemble of full length C99 in membrane and the potential role played by C99 structure in recognition and processing by γ-secretase. Taken together, these results open new paths to investigate the role of C99 structure in interactions with γ-secretase and Aβ, which may lead to new perspectives on the genesis of amyloid in AD.
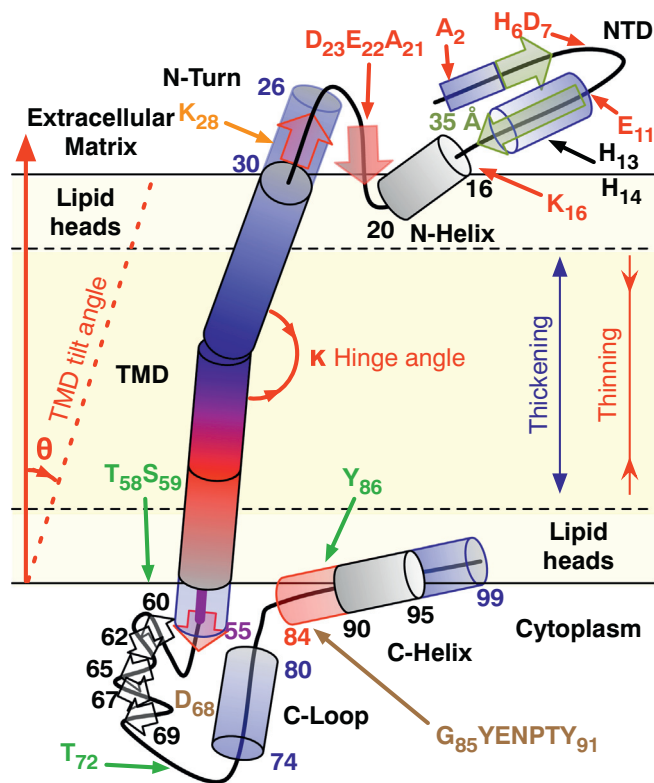
Transparency document

Acknowledgements

Fig. 7. Yellow shading represents the hydrophobic environment of the membrane. Secondary structures resulting from membrane thinning (red), membrane thickening (blue), and unique to 35 Å membranes (gold) are transparent. Residue indices are provided to identify regions in which secondary structure is observed. Residues identified with arrows identify mutations in familial AD (red), are important for metal binding (black), are phosphorylatable (green), substantially change Aβ length produced (orange), or are critical for C31 formation and cytotoxicity (brown). The TMD GG hinge angle mean and variance increase with thinning membrane. White C-loop β-strands are transient in many membrane conditions.

Appendix A. Supplementary data

Supplementary data to this article can be found online at https://doi.org/10.1016/j.bbamem.2018.04.002.

References

[1] C. Priller, T. Bauer, G. Mitteregger, B. Krebs, H.A. Kretzschmar, J. Herms, Synapse formation and function is modulated by the amyloid precursor protein, J. Neurosci. 26 (2006) 7212–7221, http://dx.doi.org/10.1523/JNEUROSCI.1450-06.2006.

[2] J. Morales-Corraliza, M.J. Mazzella, J.D. Berger, N.S. Diaz, J.H.K. Choi, E. Levy, Y. Matsuoka, E. Planel, P.M. Mathews, In vivo turnover of tau and APP metabolites in the brains of wild-type and Tg2576 mice: greater stability of sAPP in the β-amyloid depositing mice, PLoS One 4 (2009) e7134, , http://dx.doi.org/10.1371/journal.pone.0007134.

[3] T. Tomita, Molecular mechanism of intramembrane proteolysis by γ-secretase, J. Biochem. 156 (2014) 195–201, http://dx.doi.org/10.1093/jb/mvu049.

[4] U. Sengupta, A.N. Nilson, R. Kayed, The role of amyloid-β oligomers in toxicity, propagation, and immunotherapy, EBioMedicine 6 (2016) 42–49, http://dx.doi.org/10.1016/j.ebiom.2016.03.035.

[5] A. Prasansuklab, T. Tewin, Amyloidosis in Alzheimer's disease: the toxicity of

amyloid beta (A), Evid. Based Complement. Alternat. Med. 2013 (2013) 10 (doi:10.1155).

[6] R. Kayed, Common structure of soluble amyloid oligomers implies common mechanism of pathogenesis, Science 300 (2003) 486–489 (80-.), https://doi.org/10.1126/science.1079469.

[7] G.M. Shankar, S. Li, T.H. Mehta, A. Garcia-munoz, E. Nina, I. Smith, F.M. Brett, M.A. Farrell, M.J. Rowan, C.A. Lemere, C.M. Regan, D.M. Walsh, B.L. Sabatini, D.J. Selkoe, Amyloid-beta protein dimers isloated directly from Alzheimer brain impair synaptic plasticity and memory, Nat. Med. 14 (2008) 837–842, http://dx.doi.org/10.1038/nm1782.Amyloid.

[8] P.J. Barrett, Y. Song, W.D. Van Horn, E.J. Hustedt, J.M. Schafer, A. Hadziselimovic, A.J. Beel, C.R. Sanders, The amyloid precursor protein has a flexible transmembrane domain and binds cholesterol, Science 336 (2012) 1168–1171 (80-.), https://doi.org/10.1126/science.1219988.

[9] Y. Song, K.F. Mittendorf, Z. Lu, C.R. Sanders, Impact of bilayer lipid composition on the structure and topology of the transmembrane amyloid precursor C99 protein, J. Am. Chem. Soc. 136 (2014) 4093–4096, http://dx.doi.org/10.1021/ja4114374.

[10] T. Tomita, T. Iwatsubo, Structural biology of presenilins and signal peptide peptidases, J. Biol. Chem. 288 (2013) 14673–14680, http://dx.doi.org/10.1074/jbc.R113.463281.

[11] M.M. Javadpour, M. Eilers, M. Groesbeek, S.O. Smith, Helix packing in polytopic membrane proteins: role of glycine in transmembrane helix association, Biophys. J. 77 (1999) 1609–1618, http://dx.doi.org/10.1016/S0006-3495(99)77009-8.

[12] S. Kim, T.-J. Jeon, A. Oberai, D. Yang, J.J. Schmidt, J.U. Bowie, Transmembrane glycine zippers: physiological and pathological roles in membrane proteins, Proc. Natl. Acad. Sci. 102 (2005) 14278–14283, http://dx.doi.org/10.1073/pnas.0501234102.

[13] A. Panahi, A. Bandara, G.A. Pantelopulos, L. Dominguez, J.E. Straub, Specific binding of cholesterol to C99 domain of amyloid precursor protein depends critically on charge state of protein, J. Phys. Chem. Lett. 7 (2016) 3535–3541, http://dx.doi.org/10.1021/acs.jpclett.6b01624.

[14] A.J. Beel, M. Sakakura, P.J. Barrett, C.R. Sanders, Direct binding of cholesterol to the amyloid precursor protein: an important interaction in lipid-Alzheimer's disease relationships? Biochim. Biophys. Acta Mol. Cell Biol. Lipids 1801 (2010) 975–982, http://dx.doi.org/10.1016/j.bbalip.2010.03.008.

[15] Y. Song, E.J. Hustedt, S. Brandon, C.R. Sanders, Competition between homo-dimerization and cholesterol binding to the C99 domain of the amyloid precursor protein, Biochemistry 52 (2013) 5051–5064, http://dx.doi.org/10.1021/bi400735x.

[16] N. Pierrot, D. Tyteca, L. D'auria, I. Dewachter, P. Gailly, A. Hendrickx, B. Tasiaux, L. El Haylani, N. Muls, F. N'Kuli, A. Laquerrière, J.B. Demoulin, D. Campion, J.P. Brion, P.J. Courtoy, P. Kienlen-Campard, J.N. Octave, Amyloid precursor protein controls cholesterol turnover needed for neuronal activity, EMBO Mol. Med. 5 (2013) 608–625, http://dx.doi.org/10.1002/emmm.201202215.

[17] C.-D. Li, Q. Xu, R.-X. Gu, J. Qu, D.-Q. Wei, The dynamic binding of cholesterol to the multiple sites of C99: as revealed by coarse-grained and all-atom simulations, Phys. Chem. Chem. Phys. 19 (2017) 3845–3856, http://dx.doi.org/10.1039/C6CP07873G.

[18] S.M. Anderson, B.K. Mueller, E.J. Lange, A. Senes, Combination of Cα–H hydrogen bonds and van der Waals packing modulates the stability of GxxxG-mediated dimers in membranes, J. Am. Chem. Soc. 139 (2017) 15774–15783, http://dx.doi.org/10.1021/jacs.7b07505.

[19] N. Miyashita, J.E. Straub, D. Thirumalai, Y. Sugita, Transmembrane structures of amyloid precursor protein dimer predicted by replica-exchange molecular dynamics simulations, J. Am. Chem. Soc. 131 (2009) 3438–3439, http://dx.doi.org/10.1021/ja809227c.

[20] N. Miyashita, J.E. Straub, D. Thirumalai, Structures of β-amyloid peptide 1–40, 1–42, and 1–55—the 672–726 fragment of APP—in a membrane environment with implications for interactions with γ-secretase, J. Am. Chem. Soc. 131 (2009) 17843–17852, http://dx.doi.org/10.1021/ja905457d.

[21] O. Pester, P.J. Barrett, D. Hornburg, P. Hornburg, R. Pröbstle, S. Widmaier, C. Kutzner, M. Dürrbaum, A. Kapurniotu, C.R. Sanders, C. Scharnagl, D. Langosch, The backbone dynamics of the amyloid precursor protein transmembrane helix provides a rationale for the sequential cleavage mechanism of gamma-secretase, J. Am. Chem. Soc. 135 (2013) 1317–1329, http://dx.doi.org/10.1021/ja3112093.

[22] Z. Cao, J.M. Hutchison, C.R. Sanders, J.U. Bowie, Backbone hydrogen bond strengths can vary widely in transmembrane helices, J. Am. Chem. Soc. 139 (2017) 10742–10749, http://dx.doi.org/10.1021/jacs.7b04819.

[23] E. Winkler, F. Kamp, J. Scheuring, A. Ebke, A. Fukumori, H. Steiner, Generation of Alzheimer disease-associated amyloid beta 42/43 peptide by gamma-secretase can be inhibited directly by modulation of membrane thickness, J. Biol. Chem. 287 (2012) 21326–21334, http://dx.doi.org/10.1074/jbc.M112.356659.

[24] O. Holmes, S. Paturi, W. Ye, M.S. Wolfe, D.J. Selkoe, Effects of membrane lipids on the activity and processivity of purified γ-secretase, Biochemistry 51 (2012) 3565–3575, http://dx.doi.org/10.1021/bi300303g.

[25] L. Dominguez, S.C. Meredith, J.E. Straub, D. Thirumalai, Transmembrane fragment structures of amyloid precursor protein depend on membrane surface curvature, J. Am. Chem. Soc. 136 (2014) 854–857, http://dx.doi.org/10.1021/ja410958j.

[26] L. Dominguez, L. Foster, S.C. Meredith, J.E. Straub, D. Thirumalai, Structural heterogeneity in transmembrane amyloid precursor protein homodimer is a consequence of environmental selection, J. Am. Chem. Soc. 136 (2014) 9619–9626, http://dx.doi.org/10.1021/ja503150x.

[27] L. Dominguez, L. Foster, J.E. Straub, D. Thirumalai, Impact of membrane lipid composition on the structure and stability of the transmembrane domain of amyloid precursor protein, Proc. Natl. Acad. Sci. 113 (2016) E5281–E5287, http://dx.doi.org/10.1073/pnas.1606482113.

[28] S. Viswanath, L. Dominguez, L.S. Foster, J.E. Straub, R. Elber, Extension of a protein docking algorithm to membranes and applications to amyloid precursor protein dimerization, Proteins: Struct., Funct., Binf. 83 (2015) 2170–2185, http://dx.doi.org/10.1002/prot.24934.

[29] M. Audagnotto, T. Lemmin, A. Barducci, M. Dal Peraro, Effect of the synaptic plasma membrane on the stability of the amyloid precursor protein homodimer, J. Phys. Chem. Lett. 7 (2016) 3572–3578, http://dx.doi.org/10.1021/acs.jpclett.6b01721.

[30] A.J. Beel, C.K. Mobley, H.J. Kim, F. Tian, A. Hadziselimovic, B. Jap, J.H. Prestegard, C.R. Sanders, Structural studies of the transmembrane C-terminal domain of the amyloid precursor protein (APP): does APP function as a cholesterol sensor? Biochemistry 47 (2008) 9428–9446, http://dx.doi.org/10.1021/bi800993c.

[31] S. Weggen, D. Beher, Molecular consequences of amyloid precursor protein and presenilin mutations causing autosomal-dominant Alzheimer's disease, Alzheimers Res. Ther. 4 (2012) 9, http://dx.doi.org/10.1186/alzrt107.

[32] Y. Yan, T.-H. Xu, K.G. Harikumar, L.J. Miller, K. Melcher, H.E. Xu, Dimerization of the transmembrane domain of amyloid precursor protein is determined by residues around the gamma-secretase cleavage sites, J. Biol. Chem. 292 (2017) jbc.M117.789669 https://doi.org/10.1074/jbc.M117.789669.

[33] M. Dimitrov, J.R. Alattia, T. Lemmin, R. Lehal, A. Fligier, J. Houacine, I. Hussain, F. Radtke, M. Dal Peraro, D. Beher, P.C. Fraering, Alzheimers disease mutations in APP but not 3-secretase modulators affect epsilon-cleavage-dependent AICD production, Nat. Commun. 4 (2013), http://dx.doi.org/10.1038/ncomms3246.

[34] T.L. Kukar, T.B. Ladd, P. Robertson, S.A. Pintchovski, B. Moore, M.A. Bann, Z. Ren, K. Jansen-West, K. Malphrus, S. Eggert, H. Maruyama, B.A. Cottrell, P. Das, G.S. Basi, E.H. Koo, T.E. Golde, Lysine 624 of the amyloid precursor protein (APP) is a critical determinant of amyloid β peptide length, J. Biol. Chem. 286 (2011) 39804–39812, http://dx.doi.org/10.1074/jbc.M111.274696.

[35] J.H. Goo, W.J. Park, Elucidation of the interactions between C99, presenilin, and nicastrin by the split-ubiquitin assay, DNA Cell Biol. 23 (2004) 59–65, http://dx.doi.org/10.1089/104454904322745934.

[36] Y. Tian, B. Bassit, D. Chau, Y.M. Li, An APP inhibitory domain containing the Flemish mutation residue modulates γ-secretase activity for AB production, Nat. Struct. Mol. Biol. 17 (2010) 151–158, http://dx.doi.org/10.1038/nsmb.1743.

[37] L. Hendriks, C.M. van Duijn, P. Cras, M. Cruts, W. Van Hul, F. van Harskamp, A. Warren, M.G. McInnis, S.E. Antonarakis, J.-J. Martin, A. Hofman, C. Van Broeckhoven, Presenile dementia and cerebral haemorrhage linked to a mutation at codon 692 of the β–amyloid precursor protein gene, Nat. Genet. 1 (1992) 218–221, http://dx.doi.org/10.1038/ng0692-218.

[38] E. Levy, M. Carman, I. Fernandez-Madrid, M. Power, I. Lieberburg, S. van Duinen, G. Bots, W. Luyendijk, B. Frangione, Mutation of the Alzheimer's disease amyloid gene in hereditary cerebral hemorrhage, Dutch type, Science 248 (1990) 1124–1126 (80-.), https://doi.org/10.1126/science.2111584.

[39] O. Bugiani, A. Padovani, M. Magoni, G. Andora, M. Sgarzi, M. Savoiardo, A. Bizzi, G. Giaccone, G. Rossi, F. Tagliavini, An Italian type of HCHWA, Neurobiol. Aging 19 (1998) S238.

[40] C. Nilsberth, A. Westlind-Danielsson, C.B. Eckman, M.M. Condron, K. Axelman, C. Forsell, C. Stenh, J. Luthman, D.B. Teplow, S.G. Younkin, J. Näslund, L. Lannfelt, The "Arctic" APP mutation (E693G) causes Alzheimer's disease by enhanced Aβ protofibril formation, Nat. Neurosci. 4 (2001) 887–893, http://dx.doi.org/10.1038/nn0901-887.

[41] T. Tomiyama, T. Nagata, H. Shimada, R. Teraoka, A. Fukushima, H. Kanemitsu, H. Takuma, R. Kuwano, M. Imagawa, S. Ataka, Y. Wada, E. Yoshioka, T. Nishizaki, Y. Watanabe, H. Mori, A new amyloid beta variant favoring oligomerization in Alzheimer's-type dementia, Ann. Neurol. 63 (2008) 377–387, http://dx.doi.org/10.1002/ana.21321.

[42] T.J. Grabowski, H.S. Cho, J.P.G. Vonsattel, G. William Rebeck, S.M. Greenberg, Novel amyloid precursor protein mutation in an Iowa family with dementia and severe cerebral amyloid angiopathy, Ann. Neurol. 49 (2001) 697–705, http://dx.doi.org/10.1002/ana.1009.

[43] M. Citron, T. Oltersdorf, C. Haass, L. McConlogue, A.Y. Hung, P. Seubert, C. Vigo-Pelfrey, I. Lieberburg, D.J. Selkoe, Mutation of the beta-amyloid precursor protein in familial Alzheimer's disease increases beta-protein production, Nature 360 (1992) 672–674, http://dx.doi.org/10.1038/360672a0.

[44] D. Kaden, A. Harmeier, C. Weise, L.M. Munter, V. Althoff, B.R. Rost, P.W. Hildebrand, D. Schmitz, M. Schaefer, R. Lurz, S. Skodda, R. Yamamoto, S. Arlt, U. Finckh, G. Multhaup, Novel APP/Abeta mutation K16N produces highly toxic heteromeric Abeta oligomers, EMBO Mol. Med. 4 (2012) 647–659, http://dx.doi.org/10.1002/emmm.201200239.

[45] L. Zhou, N. Brouwers, I. Benilova, A. Vandersteen, M. Mercken, K. Van Laere, P. Van Damme, D. Demedts, F. Van Leuven, K. Sleegers, K. Broersen, C. Van Broeckhoven, R. Vandenberghe, B. De Strooper, Amyloid precursor protein mutation E682K at the alternative β-secretase cleavage β'-site increases Aβ generation, EMBO Mol. Med. 3 (2011) 291–302, http://dx.doi.org/10.1002/emmm.201100138.

[46] M. Oishi, A.C. Nairn, A.J. Czernik, G.S. Lim, T. Isohara, S.E. Gandy, P. Greengard, T. Suzuki, The cytoplasmic domain of Alzheimer's amyloid precursor protein is phosphorylated at Thr654, Ser655, and Thr668 in adult rat brain and cultured cells, Mol. Med. 3 (1997) 111–123 http://www.pubmedcentral.nih.gov/articlerender.fcgi?artid=2230054&tool=pmcentrez&rendertype=abstract.

[47] Y. Wakutani, K. Watanabe, Y. Adachi, K. Wada-Isoe, K. Urakami, H. Ninomiya, T.C. Saido, T. Hashimoto, T. Iwatsubo, K. Nakashima, Novel amyloid precursor protein gene missense mutation (D678N) in probable familial Alzheimer's disease, J. Neurol. Neurosurg. Psychiatry 75 (2004) 1039–1042, http://dx.doi.org/10.1136/jnnp.2003.010611.

[48] G. Di Fede, M. Catania, M. Morbin, G. Rossi, S. Suardi, G. Mazzoleni, M. Merlin, A.R. Giovagnoli, S. Prioni, A. Erbetta, C. Falcone, M. Gobbi, L. Colombo, A. Bastone, M. Beeg, C. Manzoni, B. Francescucci, A. Spagnoli, L. Cantu, E. Del Favero, E. Levy, M. Salmona, F. Tagliavini, A recessive mutation in the APP gene with dominant-negative effect on amyloidogenesis, Science 323 (2009) 1473–1477 (80-.), https://doi.org/10.1126/science.1168979.

[49] C.J. Maynard, A.I. Bush, C.L. Masters, R. Cappai, Q.-X. Li, Metals and amyloid-beta in Alzheimer's disease, Int. J. Exp. Pathol. 86 (2005) 147–159, http://dx.doi.org/10.1111/j.0959-9673.2005.00434.x.

[50] G.M. Shaked, M.P. Kummer, D.C. Lu, V. Galvan, D.E. Bredesen, E.H. Koo, Abeta induces cell death by direct interaction with its cognate extracellular domain on APP (APP 597-624), FASEB J. 20 (2006) 1246–1254, http://dx.doi.org/10.1096/fj.05-5032fje.

[51] N. Zambrano, P. Bruni, G. Minopoli, R. Mosca, D. Molino, C. Russo, G. Schettini, M. Sudol, T. Russo, The β-amyloid precursor protein APP is tyrosine-phosphorylated in cells expressing a constitutively active form of the Abl protoncogene, J. Biol. Chem. 276 (2001) 19787–19792, http://dx.doi.org/10.1074/jbc.M100792200.

[52] S.I. Vieira, S. Rebelo, S.C. Domingues, E.F. Cruz e Silva, O.A.B. Cruz e Silva, S655 phosphorylation enhances APP secretory traffic, Mol. Cell. Biochem. 328 (2009) 145–154, http://dx.doi.org/10.1007/s11010-009-0084-7.

[53] C. Feyt, N. Pierrot, B. Tasiaux, J. Van Hees, P. Kienlen-Campard, P.J. Courtoy, J.N. Octave, Phosphorylation of APP695 at Thr668 decreases gamma-cleavage and extracellular Abeta, Biochem. Biophys. Res. Commun. 357 (2007) 1004–1010, http://dx.doi.org/10.1016/j.bbrc.2007.04.036.

[54] E. Poulsen, F. Iannuzzi, H. Rasmussen, T. Maier, J. Enghild, A. Jørgensen, C. Matrone, An aberrant phosphorylation of amyloid precursor protein tyrosine regulates its trafficking and the binding to the Clathrin endocytic complex in neural stem cells of Alzheimer's disease patients, Front. Mol. Neurosci. 10 (2017) 59, http://dx.doi.org/10.3389/fnmol.2017.00059.

[55] Y. Sano, T. Nakaya, S. Pedrini, S. Takeda, K. Iijima-Ando, K. Iijima, P.M. Mathews, S. Itohara, S. Gandy, T. Suzuki, Physiological mouse brain Aβ levels are not related to the phosphorylation state of Threonine-668 of Alzheimer's APP, PLoS One 1 (2006) e51, , http://dx.doi.org/10.1371/journal.pone.0000051.

[56] T. Suzuki, M. Oishi, D.R. Marshak, A.J. Czernik, A.C. Nairn, P. Greengard, Cell cycle-dependent regulation of the phosphorylation and metabolism of the Alzheimer amyloid precursor protein, EMBO J. 13 (1994) 1114–1122.

[57] T.A. Ramelot, L.N. Gentile, L.K. Nicholson, Transient structure of the amyloid precursor protein cytoplasmic tail indicates preordering of structure for binding to cytosolic factors, Biochemistry 39 (2000) 2714–2725, http://dx.doi.org/10.1021/bi992580m.

[58] U. Giambarella, T. Yamatsuji, T. Okamoto, T. Matsui, T. Ikezu, Y. Murayama, M.A. Levine, A. Katz, N. Gautam, I. Nishimoto, G protein beta gamma complex-mediated apoptosis by familial Alzheimer's disease mutant of APP, EMBO J. 16 (1997) 4897–4907.

[59] T. Russo, R. Faraonio, G. Minopoli, P. De Candia, S. De Renzis, N. Zambrano, Fe65 and the protein network centered around the cytosolic domain of the Alzheimer's beta-amyloid precursor protein, FEBS Lett. 434 (1998) 1–7, http://dx.doi.org/10.1016/S0014-5793(98)00941-7.

[60] Z. Zhang, C.H. Lee, V. Mandiyan, J.P. Borg, B. Margolis, J. Schlessinger, J. Kuriyan, Sequence-specific recognition of the internalization motif of the Alzheimer's amyloid precursor protein by the X11 PTB domain, EMBO J. 16 (1997) 6141–6150, http://dx.doi.org/10.1093/emboj/16.20.6141.

[61] L. Parisiadou, S. Efthimiopoulos, Expression of mDab1 promotes the stability and processing of amyloid precursor protein and this effect is counteracted by X11?? Neurobiol. Aging 28 (2007) 377–388, http://dx.doi.org/10.1016/j.neurobiolaging.2005.12.015.

[62] M.H. Scheinfeld, R. Roncarati, P. Vito, P.A. Lopez, M. Abdallah, L. D'Adamio, Jun NH2-terminal kinase (JNK) interacting protein 1 (JIP1) binds the cytoplasmic domain of the Alzheimer's β-amyloid precursor protein (APP), J. Biol. Chem. 277 (2002) 3767–3775, http://dx.doi.org/10.1074/jbc.M108357200.

[63] D.C. Lu, S. Rabizadeh, S. Chandra, R.F. Shayya, L.M. Ellerby, X. Ye, G.S. Salvesen, E.H. Koo, D.E. Bredesen, A second cytotoxic proteolytic peptide derived from amyloid β-protein precursor, Nat. Med. 6 (2000) 397–404, http://dx.doi.org/10.1038/74656.

[64] D.C. Lu, S. Soriano, D.E. Bredesen, E.H. Koo, Caspase cleavage of the amyloid precursor protein modulates amyloid β-protein toxicity, J. Neurochem. 87 (2003) 733–741, http://dx.doi.org/10.1046/j.1471-4159.2003.02059.x.

[65] B. Tarus, J.E. Straub, D. Thirumalai, Dynamics of Asp23–Lys28 salt-bridge formation in Abeta 10–35 monomers, J. Am. Chem. Soc. 128 (2006) 16159–16168, http://dx.doi.org/10.1021/ja064872y.

[66] J.E. Straub, D. Thirumalai, Toward a molecular theory of early and late events in monomer to amyloid fibril formation, Annu. Rev. Phys. Chem. 62 (2011) 437–463, http://dx.doi.org/10.1146/annurev-physchem-032210-103526.

[67] N.L. Fawzi, A.H. Phillips, J.Z. Ruscio, M. Doucleff, D.E. Wemmer, T. Head-Gordon, Structure and dynamics of the Aβ 21–30 peptide from the interplay of NMR experiments and molecular simulations, J. Am. Chem. Soc. 130 (2008) 6145–6158, http://dx.doi.org/10.1021/ja710366c.

[68] Y. Sugita, Y. Okamoto, Replica exchange molecular dynamics method for protein folding simulation, Chem. Phys. Lett. 314 (1999) 141–151, http://dx.doi.org/10.1016/S0009-2614(99)01123-9.

[69] W. Im, M. Feig, C.L. Brooks, An implicit membrane generalized born theory for the study of structure, stability, and interactions of membrane proteins, Biophys. J. 85 (2003) 2900–2918, http://dx.doi.org/10.1016/S0006-3495(03)74712-2.

[70] Y. Shen, F. Delaglio, G. Cornilescu, A. Bax, TALOS+: a hybrid method for predicting protein backbone torsion angles from NMR chemical shifts, J. Biomol. NMR 44 (2009) 213–223, http://dx.doi.org/10.1007/s10858-009-9333-z.

[71] M.V. Shapovalov, R.L. Dunbrack, A smoothed backbone-dependent rotamer library

for proteins derived from adaptive kernel density estimates and regressions, Structure 19 (2011) 844–858, http://dx.doi.org/10.1016/j.str.2011.03.019.

[72] E.F. Pettersen, T.D. Goddard, C.C. Huang, G.S. Couch, D.M. Greenblatt, E.C. Meng, T.E. Ferrin, UCSF chimera - a visualization system for exploratory research and analysis, J. Comput. Chem. 25 (2004) 1605–1612, http://dx.doi.org/10.1002/jcc.20084.

[73] B.R. Brooks, C.L. Brooks, A.D. Mackerell, L. Nilsson, R.J. Petrella, B. Roux, Y. Won, G. Archontis, C. Bartels, S. Boresch, A. Caflisch, L. Caves, Q. Cui, A.R. Dinner, M. Feig, S. Fischer, J. Gao, M. Hodoscek, W. Im, K. Kuczera, T. Lazaridis, J. Ma, V. Ovchinnikov, E. Paci, R.W. Pastor, C.B. Post, J.Z. Pu, M. Schaefer, B. Tidor, R.M. Venable, H.L. Woodcock, X. Wu, W. Yang, D.M. York, M. Karplus, CHARMM: the biomolecular simulation program, J. Comput. Chem. 30 (2009) 1545–1614, http://dx.doi.org/10.1002/jcc.21287.

[74] J. Huang, A.D. MacKerell, CHARMM36 all-atom additive protein force field: validation based on comparison to NMR data, J. Comput. Chem. 34 (2013) 2135–2145, http://dx.doi.org/10.1002/jcc.23354.

[75] C.M. Siwy, C. Lockhart, D.K. Klimov, Is the conformational ensemble of Alzheimer's Aβ10–40 peptide force field dependent? PLoS Comput. Biol. 13 (2017) 1–26, http://dx.doi.org/10.1371/journal.pcbi.1005314.

[76] E. Jones, T. Oliphant, P. Peterson, et al., SciPy: Open Source Scientific Tools for Python, (n.d.). http://www.scipy.org/.

[77] S. van der Walt, S.C. Colbert, G. Varoquaux, The NumPy Array: a structure for efficient numerical computation, Comput. Sci. Eng. 13 (2011) 22–30, http://dx.doi.org/10.1109/MCSE.2011.37.

[78] S. Behnel, R. Bradshaw, C. Citro, L. Dalcin, D.S. Seljebotn, K. Smith, Cython: the best of both worlds, Comput. Sci. Eng. 13 (2011) 31–39, http://dx.doi.org/10.1109/MCSE.2010.118.

[79] J.D. Hunter, Matplotlib: a 2D graphics environment, Comput. Sci. Eng. 9 (2007) 90–95, http://dx.doi.org/10.1109/MCSE.2007.55.

[80] W. Humphrey, A. Dalke, K. Schulten, VMD – visual molecular dynamics, J. Mol. Graph. 14 (1996) 33–38.

[81] R.J. Gowers, M. Linke, J. Barnoud, T.J.E. Reddy, M.N. Melo, S.L. Seyler, D.L. Dotson, J. Domanski, S. Buchoux, I.M. Kenney, O. Beckstein, MDAnalysis: a Python Package for the Rapid Analysis of Molecular Dynamics Simulations, Proc. 15th Python Sci. Conf., Scipy, (2016), pp. 102–109 http://conference.scipy.org/proceedings/scipy2016/pdfs/oliver_beckstein.pdf.

[82] N. Michaud-Agrawal, E.J. Denning, T.B. Woolf, O. Beckstein, MDAnalysis: a toolkit

[83] R.T. McGibbon, K.A. Beauchamp, M.P. Harrigan, C. Klein, J.M. Swails, C.X. Hernández, C.R. Schwantes, L.P. Wang, T.J. Lane, V.S. Pande, MDTraj: a modern open library for the analysis of molecular dynamics trajectories, Biophys. J. 109 (2015) 1528–1532, http://dx.doi.org/10.1016/j.bpj.2015.08.015.

[84] B. Han, Y. Liu, S.W. Ginzinger, D.S. Wishart, SHIFTX2: significantly improved protein chemical shift prediction, J. Biomol. NMR 50 (2011) 43–57, http://dx.doi.org/10.1007/s10858-011-9478-4.

[85] A. Altis, P.H. Nguyen, R. Hegger, G. Stock, Dihedral angle principal component analysis of molecular dynamics simulations, J. Chem. Phys. 126 (2007) 1–10, http://dx.doi.org/10.1063/1.2746330.

[86] A.P. Dempster, N.M. Laird, D.B. Rubin, Maximum likelihood from incomplete data via the EM algorithm, J. R. Stat. Soc. Ser. B 39 (1977) 1–38 http://www.jstor.org/stable/2984875.

[87] T. Mori, N. Miyashita, W. Im, M. Feig, Y. Sugita, Molecular dynamics simulations of biological membranes and membrane proteins using enhanced conformational sampling algorithms, Biochim. Biophys. Acta Biomembr. 1858 (2016) 1635–1651, http://dx.doi.org/10.1016/j.bbamem.2015.12.032.

[88] N. Kučerka, M.P. Nieh, J. Katsaras, Fluid phase lipid areas and bilayer thicknesses of commonly used phosphatidylcholines as a function of temperature, Biochim. Biophys. Acta Biomembr. 1808 (2011) 2761–2771, http://dx.doi.org/10.1016/j.bbamem.2011.07.022.

[89] S. Vivekanandan, J.R. Brender, S.Y. Lee, A. Ramamoorthy, A partially folded structure of amyloid-beta(1–40) in an aqueous environment, Biochem. Biophys. Res. Commun. 411 (2011) 312–316, http://dx.doi.org/10.1016/j.bbrc.2011.06.133.

[90] D.J. Lindberg, E. Wesén, J. Björkeroth, S. Rocha, E.K. Esbjörner, Lipid membranes catalyse the fibril formation of the amyloid-β (1–42) peptide through lipid-fibril interactions that reinforce secondary pathways, Biochim. Biophys. Acta Biomembr. 1859 (2017) 1921–1929, http://dx.doi.org/10.1016/j.bbamem.2017.05.012.

[91] S. Furlan, C. Hureau, P. Faller, G. La Penna, Modeling the Cu$^+$ binding in the 1–16 region of the amyloid-β(1–40) involved in Alzheimer's disease, J. Phys. Chem. B 114 (2010) 15119–15133, http://dx.doi.org/10.1021/jp102928h.

[92] S. Furlan, C. Hureau, P. Faller, G. La Penna, Modeling copper binding to the amyloid-β peptide at different pH: toward a molecular mechanism for cu reduction, J. Phys. Chem. B 116 (2012) 11899–11910, http://dx.doi.org/10.1021/jp308977s.